Advances in Water Resources 70 (2014) 172–184

Contents lists available at ScienceDirect

Advances in Water Resources

journal homepage: www.elsevier.com/locate/advwatres

Analytical solutions for benchmarking cold regions subsurface water flow and energy transport models: One-dimensional soil thaw with conduction and advection

Barret L. Kurylyk [a,*], Jeffrey M. McKenzie [b], Kerry T.B. MacQuarrie [a], Clifford I. Voss [c]

[a] Department of Civil Engineering, University of New Brunswick, Fredericton, NB, Canada
[b] Department of Earth and Planetary Sciences, McGill University, Montreal, QC, Canada
[c] U.S. Geological Survey, Menlo Park, CA, USA

ARTICLE INFO

Article history:
Received 11 February 2014
Received in revised form 11 May 2014
Accepted 13 May 2014
Available online 21 May 2014

Keywords:
Analytical solutions
Thawing front
Phase change
Thermohydraulic models
Stefan problem
Freezing and thawing

ABSTRACT

Numerous cold regions water flow and energy transport models have emerged in recent years. Dissimilarities often exist in their mathematical formulations and/or numerical solution techniques, but few analytical solutions exist for benchmarking flow and energy transport models that include pore water phase change. This paper presents a detailed derivation of the Lunardini solution, an approximate analytical solution for predicting soil thawing subject to conduction, advection, and phase change. Fifteen thawing scenarios are examined by considering differences in porosity, surface temperature, Darcy velocity, and initial temperature. The accuracy of the Lunardini solution is shown to be proportional to the Stefan number. The analytical solution results obtained for soil thawing scenarios with water flow and advection are compared to those obtained from the finite element model SUTRA. Three problems, two involving the Lunardini solution and one involving the classic Neumann solution, are recommended as standard benchmarks for future model development and testing.

1. Introduction

A number of powerful simulators of cold regions subsurface water flow and energy transport have emerged in recent years e.g., [1–16]. These models, most of which are briefly described by Kurylyk and Watanabe [17], simulate subsurface energy exchange via conduction, advection and pore water phase change and account for reduction in hydraulic conductivity due to pore ice formation e.g., [17–21]. Researchers have employed these models to quantify the subsurface hydrological and thermal influences of climate change in cold regions. Simulated and/or observed climate change impacts in cryogenic soils include permafrost degradation, active layer expansion, talik formation, dormant aquifer activation, and changes to the timing, magnitude, and temperature of groundwater recharge and discharge [22–29]. Three other emerging applications of cold regions subsurface flow and heat transport models are to aid in the design and analysis of frozen soil barriers to impede the migration of contaminated water [30], to simulate the influence of design alternatives for cold regions infrastructure [31], and to investigate hypothetical hydrological processes on Mars [2,32].

These cold regions models are characterized by diversity in both their nomenclature and underlying theory due to the differing backgrounds of researchers in this multi-disciplinary field. These variations elicit the demand for benchmarking problems to test the physics and numerical schemes of these models and to conduct inter-code comparisons. These benchmarking problems can be formulated from existing analytical solutions or developed from well-posed numerical problems [4]. For example, groundwater flow and energy transport models that include the dynamic freeze–thaw process have been tested against analytical solutions, such as the Neumann or Stefan solutions [33], which predict the propagation of soil thawing or freezing by considering subsurface heat exchange through conduction and pore water phase change. These classic solutions do not accommodate advective heat transport and are therefore limited in their ability to fully test numerical models that include subsurface heat transfer due to groundwater flow. Indeed the inclusion of heat advection via subsurface water flow is one primary advantage of many of these emerging models in comparison to simpler conduction-based cold regions heat transport models e.g., [34,35].

* Corresponding author. Address: Department of Civil Engineering, UNB, 17 Dineen Drive, P.O. Box 4400, Fredericton, NB E3B 5A3, Canada. Tel.: +1 506 453 4521.
E-mail address: barret.kurylyk@unb.ca (B.L. Kurylyk).

http://dx.doi.org/10.1016/j.advwatres.2014.05.005
0309-1708/

To the authors' knowledge, no numerical models of subsurface water flow and heat transport have been compared to analytical solutions that consider heat exchange due to conduction, advection, and pore water phase change. Exact analytical solutions that include advection have been proposed for soil thawing problems [36,37], but these solutions are only valid if the pore water velocity is proportional to the thawing front penetration rate. This physical scenario is difficult to simulate given the Darcian approaches employed in most existing numerical models e.g., [1,4], and thus these exact solutions have not been utilized for benchmarking purposes. A more general approximate analytical solution has also been proposed by Lunardini [37] to estimate one-dimensional soil thawing subject to advection, conduction, and phase change. This solution has received very little attention in hydrological literature to date, which may be due in part to the geotechnical engineering nomenclature employed, the lack of a detailed description of the solution's mathematical development and inherent limitations, and the approximate nature of the solution.

The objectives of the present contribution are fivefold:

1. To present the governing equations, initial conditions, and boundary conditions for the classic Stefan and Neumann solutions for soil thawing.
2. To detail the formulation of Lunardini's [37] approximate solution in conventional hydrological nomenclature.
3. To determine the accuracy of this solution in the case of negligible water flow via comparison to the exact Neumann solution.
4. To assess the accuracy of this solution in the case of high water flow and heat advection via comparisons to results from a numerical model, and
5. To choose three thawing scenarios to serve as benchmark problems for cold regions groundwater flow and energy transport models.

We begin by first presenting the form and application of the classic Stefan and Neumann solutions [38], which are the basis for the development and application of the approximate solution developed by Lunardini [37]. This approximate solution [37] shall hereafter be referred to as the 'Lunardini solution', although we recognize that Lunardini developed and synthesized numerous analytical solutions for cold regions soils [33,39]. The mathematical development of the Lunardini solution is presented in far more detail than in the original formulation to enable others to adapt it for their own research purposes. The influence of soil conditions (e.g., porosity and surface temperature) on the accuracy of the Lunardini solution is assessed by setting the Darcy velocity, and hence the heat advection, to a very low value and comparing the results to those obtained from the exact Neumann solution. Because the Neumann solution does not accommodate advection, Lunardini solution results with high water flow rates are compared to results obtained from a numerical model of coupled water flow and heat transport with phase change. Of these numerous simulations, three particular thawing scenarios are selected and presented in sufficient detail to serve as viable benchmarks. We anticipate that these problems will be an important contribution to the ambitious benchmarking project proposed by Grenier et al. [40] for comparing cold regions thermo-hydraulic codes.

2. Analytical solutions

2.1. Stefan solution

Early geotechnical engineering solutions for estimating frost penetration depth in soils were derived from the seminal research of Stefan [41] who focused on freezing and thawing of sea ice [33]. Consequently, problems involving the movement of a freezing or thawing front are often referred to as 'Stefan problems'. Various forms of the Stefan solution have been proposed in literature [42]; herein we briefly describe the development of a simple form of the Stefan solution, which calculates the penetration of the thawing front into an initially frozen, thermally uniform, semi-infinite column of soil as a result of a sudden increase in surface temperature (Fig. 1). Heat exchange occurs only due to conduction and pore water phase change. Soil thawing is assumed to occur over an infinitesimal temperature range, thus the soil at any point in space and time is considered either frozen or thawed, although trace amounts of unfrozen residual water may remain within the frozen section (Fig. 1).

The transient, one dimensional conduction equation is the governing heat transfer equation that represents temperature dynamics within the thawed zone of the thawing soil:

$$\lambda \frac{\partial^2 T}{\partial x^2} = c\rho \frac{\partial T}{\partial t} \quad \text{for } 0 \leqslant x \leqslant X \tag{1}$$

where λ is the bulk thermal conductivity of the thawed zone (W m^{-1} °C), c is the specific heat of the thawed medium (soil water matrix, J kg^{-1} °C^{-1}), ρ is the density of the thawed zone (kg m^{-3}), x is the distance below the surface for any arbitrary point (m), T is the temperature distribution in the thawed zone (°C), t is time (s), and X is the distance between the surface and the interface between the thawed and frozen zones (m) (Fig. 1).

For the Stefan solution, the boundary and initial conditions are:

$$\text{Initial conditions}: T(x, t = 0) = T_f \tag{2}$$

$$\text{Surface boundary condition}: T(x = 0, t) = T_s \tag{3}$$

$$\text{Interface boundary condition}: T(x = X, t) = T_f \tag{4}$$

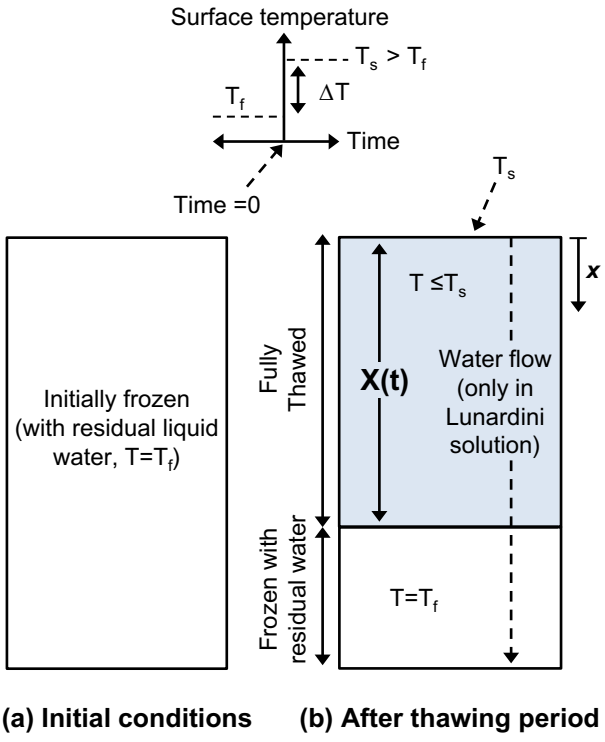

Fig. 1. The theoretical conditions represented by the analytical solutions of Stefan (Eq. (6)), Neumann (with initial conditions at the freezing temperature, Eqs. (12), (13) and (15)) and Lunardini (Eq. (33)) for (a) time = 0, and (b) after a period of soil thawing. Note the difference between x (distance below surface for any arbitrary point) and X (distance below surface to freeze–thaw interface). X increases with time. The water flow (heat advection) indicated in (b) is not included in the Stefan or Neumann solutions (adapted from [37,50]).

where T_f is the temperature at which all soil freezing or thawing occurs (taken as 0 °C) and T_s is the prescribed surface temperature boundary condition (>0 °C) (Fig. 1). As Eq. (2) indicates, the initial temperature of the soil is exactly at the soil freezing temperature. Thus the soil is initially frozen, but any increase in temperature will result in fully thawed conditions. This also implies that when $x > X$ (i.e., within the frozen zone) at any point in time, the temperature is uniform and equal to the freezing temperature (Fig. 1). This condition simplifies the medium thermal dynamics, because conductive heat transfer will never occur in the frozen zone due to the absence of a thermal gradient. As such, only the thermal properties of the thawed zone have to be considered (Eq. (1)).

At the thawing front, the conductive heat flux is equal to the rate of latent energy absorbed due to soil thawing:

$$-\lambda \frac{\partial T(X,t)}{\partial x} = S_{wf}\rho_w \varepsilon L_f \frac{dX}{dt} \tag{5}$$

where S_{wf} is the liquid water saturation in the thawed zone that was originally frozen (volume of ice that undergoes thawing divided by pore volume), ρ_w is the liquid water density (kg m^{-3}), ε is the soil porosity, and L_f is the latent heat of fusion for water (334,000 J kg^{-1}, [4]). The notation employed on the right hand side of Eq. (5) indicates that the temperature gradient is evaluated at the freezing front.

Lunardini [33] and Jumikis [38] detail different approaches for obtaining the Stefan solution to the governing equations (Eqs. (1) and (5)) subject to the conditions given in Eqs. (2)–(4). Both approaches explicitly or implicitly assume that the temperature distribution in the thawed zone is linear. This implies that the propagation rate of the thawing front is sufficiently slow to allow the thermal regime within the thawed zone to achieve steady state conditions at any point in time (i.e., the right hand side of Eq. (1) = 0). Thus, the resultant Stefan solution is an approximate solution to Eqs. (1) and (5) subject to the initial and boundary conditions (Eqs. (2)–(4)) given that the position of the thawing front is continuously moving downwards, and thus the thermal regime of the thawed zone has not generally attained true steady-state.

Under this steady-state assumption, the Stefan solution, which calculates the location of the thawing front (X, Fig. 1) as a function of time, can be shown to be [38]:

$$X = \sqrt{2 S_T \alpha t} \tag{6}$$

where α is the thermal diffusivity of the thawed medium (thermal conductivity divided by volumetric heat capacity, m^2 s^{-1}) and S_T is the dimensionless Stefan number, which is the ratio of sensible heat to latent heat. For the case presented in Fig. 1, S_T can be shown to be:

$$S_T = \frac{c\rho\,(T_s - T_f)}{S_{wf}\,\rho_w\,\varepsilon\,L_f} = \frac{\lambda\,T_s}{\alpha S_{wf}\,\rho_w\,\varepsilon\,L_f} \tag{7}$$

where all terms have been previously defined. It is reasonable to suppose that the linear temperature distribution assumption of the Stefan equation is most valid when the Stefan number is low. In this case, the thawing front penetrates slowly, and the thawed zone temperature profile approaches steady-state conditions.

All of the analytical solutions discussed in this paper tacitly assume that the density of ice is equivalent to the density of water, and thus there is no change in volume as a result of phase change. Also, all of the analytical solutions and most of the numerical models listed in the present study ignore heat transport through the gas phase, although two recent numerical models have considered three phase heat transport in cryogenic soils [2,12]. Finally, it should be noted that the soil water saturation that has undergone phase change (S_{wf}) is equal to the liquid water saturation in the thawed zone minus the residual water saturation in the frozen zone (i.e., the remaining liquid water when the soil is frozen, Fig. 1). Thus, in the case of fully saturated soils with very small residual water saturations (e.g., 0.0001), S_{wf} can be effectively taken as 1.0. This simplification was employed for all of the analytical solution results presented in this study.

2.2. Neumann solution

Neumann [43] presented an exact solution for the freezing of bulk water that predates the Stefan solution, but it was not widely disseminated until half a century after its development [33]. This exact solution, when applied for the purpose of simulating thaw penetration in porous media, relaxes two of the assumptions of the Stefan solution presented above: the initial temperature in the domain may be below the freezing temperature, and the temperature distribution within the thawed zone is generally non-linear [38]. Because the Neumann solution allows for initial temperatures below the freezing temperature, the resultant thermal gradient from the thawing front towards the frozen zone will induce frozen zone conductive heat transfer. The thawed and frozen zones are characterized by different thermal properties, and thus two distinct transient heat conduction equations are considered:

$$\alpha \frac{\partial^2 T}{\partial x^2} = \frac{\partial T}{\partial t} \quad \text{for } 0 \leqslant x \leqslant X \tag{8a}$$

$$\alpha_f \frac{\partial^2 \overline{T}}{\partial x^2} = \frac{\partial \overline{T}}{\partial t} \quad \text{for } X \leqslant x \leqslant \infty \tag{8b}$$

where $\overline{T}$ is the temperature distribution in the frozen zone (°C), α_f is the bulk thermal diffusivity of the frozen zone (m^2 s^{-1}), and all other parameters are defined the same as in the case of the Stefan solution. Eq. (8a) is identical to Eq. (1) and represents thermal dynamics in the thawed zone, whereas Eq. (8b) represents thermal dynamics in the frozen zone.

The surface and interface boundary conditions are the same as for the Stefan solution (Eqs. (3) and (4)). Note that the thawed and frozen zone temperature distributions (T and $\overline{T}$) converge at the interface in accordance with Eq. (4). The initial conditions for the Neumann solution can be expressed more generally than those for the Stefan solution:

$$\text{Initial conditions}: \quad T(x, t = 0) = T_i \tag{9}$$

where T_i is the uniformly distributed initial temperature (<0 °C). The Neumann solution is also subject to a bottom boundary condition.

$$\text{Bottom boundary condition}: \quad T(x = \infty, t) = T_i \tag{10}$$

The interface energy balance becomes more complex than in the case of the Stefan solution development (Eq. (5)), because the conductive flux into the frozen zone must also be considered:

$$-\lambda \frac{\partial T(X,t)}{\partial x} = S_{wf}\rho_w \varepsilon L_f \frac{dX}{dt} - \lambda_f \frac{\partial \overline{T}(X,t)}{\partial x} \tag{11}$$

where λ_f is the bulk thermal conductivity of the frozen zone (W m^{-1} °C^{-1}). Eq. (11) essentially states that the conductive energy flux at the interface from the thawed zone is equal to the rate of energy absorbed due to soil thawing plus the conductive energy flux from the interface to the frozen zone.

Several cold regions geotechnical engineering texts e.g., [33,38,39,44,45] present derivations of the Neumann solution to the governing equations (Eqs. (8a), (8b) and (11)) subject to the boundary and initial conditions (Eqs. (3), (4), (9) and (10)). The Neumann solution is typically expressed with parameters employed in geotechnical engineering, but it is presented here in conventional hydrology nomenclature:

$$X = m\sqrt{t} \tag{12}$$

where m is the coefficient of proportionality (m s$^{-0.5}$), which can be found by equating Y_1 and Y_2:

$$Y_1 = 0.5 L_f S_{wf} \rho_w \varepsilon \sqrt{\pi} m \tag{13}$$

$$Y_2 = \frac{\lambda}{\sqrt{\alpha}}(T_s - T_f)\left\{\exp\left(\frac{-m^2}{4\alpha}\right)\Big/\operatorname{erf}\left(\frac{m}{2\sqrt{\alpha}}\right)\right\} - \frac{\lambda_f}{\sqrt{\alpha_f}}(T_i - T_f)\left\{\exp\left(\frac{-m^2}{4\alpha_f}\right)\Big/\operatorname{erfc}\left(\frac{m}{2\sqrt{\alpha_f}}\right)\right\} \tag{14}$$

where erf is the error function, erfc is the complementary error function, and other terms have been previously defined.

This exact solution can be compared to the approximate Stefan solution by setting the initial temperature of the medium at the freezing temperature ($T_i = T_f = 0$ °C). For this simplified scenario (Fig. 1), conduction only occurs within the expanding thawed zone as there is no thermal gradient below the thawing front. In this case, Y_1 remains the same, and Y_2 simplifies to:

$$Y_2 = \frac{\lambda}{\sqrt{\alpha}}(T_s - T_f)\left[\exp\left(\frac{-m^2}{4\alpha}\right)\Big/\operatorname{erf}\left(\frac{m}{2\sqrt{\alpha}}\right)\right] \tag{15}$$

The Neumann solution can also be applied to calculate the temperature distributions in the thawed and frozen zones or to simulate the propagation of a freezing front e.g., [33,38,39,46]. However, for the purpose of comparison to the Stefan and Lunardini solutions, we focus on the application of the solution to predict the depth to the thawing front (Eq. (12)).

Several variations on the Neumann and Stefan solutions have been proposed that accommodate harmonic or irregular surface temperature boundary conditions, multi-layered soils, temperature-dependent thermal conductivity, and heat transfer coefficients between the lower atmosphere and ground surface e.g., [39,47–52]. For example, McKenzie et al. [4] utilized an analytical solution to a physical scenario similar to that shown in Fig. 1, but with a partially frozen zone between the thawed and frozen zones to test the performance of the cold regions thermo-hydraulic model SUTRA. This solution is not described in the present article, as its application as a numerical model benchmark has been previously detailed by McKenzie et al. [4] and because it does not accommodate heat advection and also invokes the limiting assumption that thermal diffusivity in the partially frozen zone is constant. In general, researchers have proposed modifications to the Stefan or Lunardini solutions to improve their fidelity to physical processes. However, these modifications, which typically introduce increased complexities into the boundary conditions or thermal properties, do not typically enhance the solutions' ability to assess the performance of the physics and numerical solution schemes of cold regions numerical models. The Neumann and Stefan solutions presented herein are the forms most commonly employed, and they have been used for making comparisons to results obtained from numerical models that include the dynamic freeze–thaw process [6,52].

2.3. Lunardini solution

Lunardini [37] produced a solution to the one-dimensional, semi-infinite soil thawing problem that is shown in Fig. 1, but, unlike the Neumann and Stefan solutions, it accommodates heat advection via water flow. Due to the principle of continuity and the one-dimensional assumptions employed in this solution, the water flux depicted in Fig. 1(b) must be the same in both the thawed and frozen zone. This assumption does not generally reflect reality given that vertical water flux is typically reduced in the frozen zone due to the hydraulic impedance of ice [17]. However, this does not limit the application of this solution for benchmarking purposes. Within the frozen zone, the water flux is still occurring in the liquid phase due to the presence of residual liquid moisture (Fig. 1). The pore ice acts to reduce the effective porosity of the soil, and thus the pore water velocity (Darcy velocity divided by effective porosity for saturated soils) will substantially increase in the frozen zone in comparison to the thawed zone. However, the advective heat flux is proportional to the Darcy velocity (flux) not the pore water velocity *per se*, and thus the increase in pore water velocity is immaterial from a heat transport point of view, at least when isothermal conditions between the ice, residual water, and soil grains are assumed.

The Lunardini solution is herein developed by first introducing the one-dimensional, transient conduction–advection equation without phase change [53,54]:

$$\lambda\frac{\partial^2 T}{\partial x^2} - v c_w \rho_w \frac{\partial T}{\partial x} = c\rho\frac{\partial T}{\partial t} \quad \text{for } 0 \leqslant x \leqslant X \tag{16}$$

where v is the Darcy velocity of the pore water (positive downwards, m s^{-1}), c_w is the specific heat of water (J kg^{-1} °C^{-1}), and other terms have been previously defined. Eq. (16) represents temperature dynamics within the upper thawed zone where energy is conducted and advected from the specified surface temperature boundary condition and converted to sensible heat via an increase in the temperature of the soil–water matrix. This equation does not account for latent heat and assumes that thermal conductivity and heat capacity are spatiotemporally invariant. Thus even for homogeneous soil, Eq. (16) is only valid in the case of constant water saturation and phase (i.e., in the thawed zone). This can be rewritten in a form closer to that of the classic advection–dispersion equation for contaminant transport e.g., [55]:

$$\alpha\frac{\partial^2 T}{\partial x^2} - v_t\frac{\partial T}{\partial x} = \frac{\partial T}{\partial t} \quad \text{for } 0 \leqslant x \leqslant X \tag{17}$$

Lunardini [33] incorrectly states that v_t (m s^{-1}) represents the velocity of the mass flux, but it actually represents the velocity of the thermal plume in the case of pure heat advection (i.e., without conduction) [56]. Under advection-dominated conditions, the thermal plume will not typically migrate at the same rate as the Darcy velocity because the volumetric heat capacity of the soil–water matrix is typically less than the volumetric heat capacity of water. In general for advection-dominated conditions, the thermal plume velocity is typically higher than the Darcy velocity but less than the pore water velocity [56]. The actual expression for v_t can be obtained by a comparison of (16) and (17):

$$v_t = v\frac{c_w\rho_w}{c\rho} \tag{18}$$

Note that it is mathematically and physically tenable to have vertically upwards Darcy velocity, but we restrict our results and discussion to vertically downwards flow given that this is the scenario that would typically occur during snowmelt, infiltration, and associated soil thaw.

The Lunardini solution is subject to the same initial conditions (Eq. (2)), surface boundary condition (Eq. (3)), and interface boundary condition (Eq. (4)) as the Stefan solution. Thus, like the Stefan solution, the medium is initially at the frozen temperature T_f (0 °C), and no conductive heat transfer ever occurs within the frozen zone due to the absence of a thermal gradient. Consequently, only the thermal properties of the thawed zone must be considered (Eq. (16)). Also, as in the case of the Stefan and Neumann solutions, the surface temperature T_s (°C) is instantaneously increased above the freezing temperature at $t = 0$ (Eq. (3)). Finally, the temperature at the boundary between the thawed and frozen zones (X, Fig. 1) is equal to the freezing temperature T_f (Eq. (4)).

The Lunardini solution energy balance at the interface between the thawed and frozen zones is expressed by equating the sum of

the conductive and advective thermal fluxes at the thawing front to the rate of latent energy absorbed at the thawing front:

$$-\lambda\frac{\partial T(X,t)}{\partial x}+vc_w\rho_w T(X,t)=S_{wf}\rho_w\varepsilon L_f\frac{dX}{dt} \tag{19}$$

The temperature at the thawing front $T(X,t)$ is 0 °C (Eq. (4)), thus the advective flux term at the thawing front is zero when the temperature scale is Celsius. Hence, Eq. (19) can be simplified and rearranged to isolate for the temperature gradient at the freezing front:

$$\frac{\partial T(X,t)}{\partial x}=-\frac{S_{wf}\rho_w\varepsilon L_f}{\lambda}\frac{dX}{dt} \tag{20}$$

It should be noted that Eq. (20) and other equations within this contribution often differ from the few equations presented in the original study [37] due to differences in the definitions of latent heat employed by geotechnical engineers and hydrologists.

Lunardini [37] presented three distinct approaches for solving the governing equations (Eqs. (17) and (20)) subject to the initial conditions (Eq. (2)) and boundary conditions (Eqs. (3) and (4)). The first approach results in an exact solution that is limited to cases where the Darcy velocity and the thermal plume velocity are proportional to the rate of the propagation of the thawing front. As previously noted, this exact solution is not well-suited for benchmarking numerical models due to this limiting condition. The second approach utilizes the heat balance integral method to obtain an approximate solution to predict the thawing front penetration. This solution approach allows the Darcy velocity to be any value, but it invokes the assumption that the temperature distribution in the thawed zone is always linear. This approach tacitly assumes that the thermal regime of the thawed zone is conduction-dominated and at steady-state. Thus, there is an implicit self-contradiction in this approach at higher Darcy velocities, as the resultant high advection rates can invalidate the assumption of conduction-dominated conditions and produce non-linear temperature profiles.

The third approach, which we employ in the present study, assumes that the rate of the thawing front propagation is slow enough to allow for steady-state temperature conditions to be achieved above the thawing front. However, the solution allows for nonlinear temperature profiles in the thawed zone due to the influence of heat advection. Thus this solution approach relaxes one of the assumptions of the second approach. It should be noted that Lunardini's [37] third approach was heavily influenced by the seminal work of Fel'dman [57].

If steady-state thermal conditions are assumed for the thawed zone, the transient governing equation (17) can be replaced with the steady-state conduction advection equation:

$$\alpha\frac{d^2T}{dx^2}-v_t\frac{dT}{dx}=0 \tag{21}$$

For a given X (Fig. 1), the solution to Eq. (21) subject to the boundary conditions at the ground surface and the thawing front (Eqs. (3) and (4)) is a special case of the classic steady-state conduction-advection solution proposed by Bredehoeft and Papadopulos [58].

For notational convenience, two new terms can be defined:

$$\gamma=\frac{dT}{dx} \tag{22}$$

$$\beta=\frac{v_t}{\alpha} \tag{23}$$

where γ is the temperature gradient at any point in the thawed zone assuming steady-state conditions (°C m^{-1}) and β is the ratio of the thermal plume velocity to the thermal diffusivity (m^{-1}). Inserting Eqs. (22) and (23) into Eq. (21) and rearranging yields:

$$\frac{d\gamma}{\gamma}=\beta\,dx \tag{24}$$

which can be solved by integrating both sides between any arbitrary x and the thawing front position X:

$$\int_{\gamma(x=x)}^{\gamma(x=X)}\frac{d\gamma}{\gamma}=\int_x^X\beta\,dx \tag{25}$$

The resultant equation for the steady-state temperature gradient can be found by performing the integrations, isolating for γ, and substituting back in the definition for γ (Eq. (22)):

$$\frac{dT}{dx}=\frac{dT(X,t)}{dx}\exp\{\beta(x-X)\} \tag{26}$$

Eq. (26) can now be rearranged and integrated from the surface ($x=0$) to the thawing front ($x=X$). The temperature gradient at the thawing front can be considered independent of the integration on the right hand side given that it is constant with respect to space:

$$\int_{T(x=0)}^{T(x=X)}dT=\frac{dT(X,t)}{dx}\int_0^X\exp\{\beta(x-X)\}\,dx \tag{27}$$

This integration can be performed by recalling that the temperatures at the surface and thawing front are T_s and 0 °C, respectively:

$$T_s=-\frac{dT(X,t)}{dx}\left\{\frac{1}{\beta}(1-\exp(-\beta X))\right\} \tag{28}$$

Eq. (28) can be rearranged to isolate for the temperature gradient at the thawing front:

$$\frac{dT(X,t)}{dx}=\frac{-T_S\beta}{\{1-\exp(-\beta X)\}} \tag{29}$$

This thawing front temperature gradient, which was obtained by solving the steady-state conduction-advection equation, can be equated to the thawing front temperature gradient obtained from the interface energy balance (Eq. (20)):

$$\frac{-T_S\beta}{(1-\exp(-\beta X))}=-\frac{S_{wf}\rho_w\varepsilon L_f}{\lambda}\frac{dX}{dt} \tag{30}$$

The rate of thawing front penetration can be isolated, and the fundamental definitions for β (Eq. (23)) and the Stefan number (Eq. (7)) can be utilized to yield:

$$\frac{dX}{dt}=\frac{v_tS_T}{\{1-\exp(-\beta X)\}} \tag{31}$$

This ordinary differential equation can be solved via a separation of variables and integrating from $t=0$ to any arbitrary t:

$$\int_{X(t=0)}^{X(t=t)}\{1-\exp(-\beta X)\}\,dX=\int_0^t v_tS_T\,dt \tag{32}$$

Both sides of Eq. (32) can be integrated to yield the implicit equation for X presented by Lunardini [37]:

$$X+\frac{\alpha}{v_t}\left\{\exp\left(-\frac{v_tX}{\alpha}\right)-1\right\}=v_tS_Tt \tag{33}$$

Eq. (33) is herein referred to as the 'Lunardini solution'. Lunardini solution inaccuracies arise due to the invoked steady-state assumption (Eq. (21)). Thawing scenarios with high Stefan numbers will experience rapid thawing front propagation and thus violate this steady-state assumption. Herein, the sensitivity of the Lunardini solution accuracy to the Stefan number is investigated

in detail by setting the Darcy velocity (and thus v_t, Eq. (18)) very low and comparing the Lunardini solution results to those of the exact Neumann solution with initial temperatures at the freezing temperature. A range of Stefan numbers is obtained by considering thawing scenarios with varying porosities and surface temperatures. This approach does not test the ability of the Lunardini solution to correctly accommodate advective heat transport. However, a comparison to the Neumann solution does indicate how inaccuracies associated with the steady-state temperature assumption influence the Lunardini solution accuracy. Furthermore, Lunardini solution results obtained for scenarios with high Darcy velocities will be compared to numerical modeling results to demonstrate the influence of heat advection on soil thawing.

Because both the Lunardini and Stefan solutions assume quasi-steady conditions, the Lunardini solution should approach the Stefan solution as advection becomes negligible. The second order Maclaurin series expansion for the exponential term in Eq. (33) through second order is [59]:

$$\exp\left(-\frac{v_t X}{\alpha}\right) \approx 1 - \frac{v_t X}{\alpha} + \frac{1}{2}\frac{v_t^2 X^2}{\alpha^2} \tag{34}$$

Higher order Maclaurin series terms will become negligible as the coefficient in the exponential term becomes smaller. This is the case as the thermal plume velocity v_t (and thus the Darcy velocity) approaches zero. In this case, Eq. (34) can be inserted into Eq. (33) to yield:

$$X + \frac{\alpha}{v_t}\left(1 - \frac{v_t X}{\alpha} + \frac{1}{2}\frac{v_t^2 X^2}{\alpha^2} - 1\right) = v_t S_T t \tag{35}$$

As expected in this case, this equation can be shown to simplify to the Stefan equation (Eq. (6)) via a cancelation of terms.

2.4. Thermal Peclet number

The relative thermal effects of advection and conduction vary temporally in the situation depicted in Fig. 1. This variability can be quantified via the dimensionless thermal Peclet number (P_e), which is the ratio of heat advection to conduction [60]:

$$P_e = \frac{v c_w \rho_w T}{-\lambda\, \partial T/\partial x} \tag{36}$$

The average thermal gradient in the thawed zone is $-T_s/X$, and the average temperature in the thawed zone is $\sim T_s/2$. Thus the average thermal Peclet number in the thawed zone can be approximated as:

$$\overline{P_e} \approx \frac{v c_w \rho_w X}{2\lambda} \tag{37}$$

Thus, for a given soil, the Peclet number for the scenario shown in Fig. 1 is dependent on the Darcy velocity and the depth to the thawed zone. It is interesting to note that this Peclet number does not directly depend on the surface temperature (T_s); however there is an indirect dependence given that the location of the thawing front (X) is influenced by T_s. The Peclet number dependence on X arises because at the initiation of soil thawing, the thermal gradient between the surface and thawing front is very high, and conduction dominates. This thermal gradient decreases with time given that the depth to the thawing front increases while the temperature difference between the surface and the thawing front is constant. Hence, the relative influences of heat advection increase with time.

3. Numerical methods

To demonstrate the utility of the Lunardini solution for benchmarking purposes, results obtained from the Lunardini solution are compared to simulations performed with the U.S. Geological Survey groundwater flow and heat transport model SUTRA [61]. SUTRA is a robust finite element model that accommodates variably saturated, multi-dimensional groundwater flow and coupled energy transport. Code modifications allow for pore water freeze–thaw in saturated environments [4]. More recently, SUTRA has been further modified to accommodate variably saturated freezing and thawing, and this version of the code has been applied to investigate coupled groundwater flow and heat transport in perennially and seasonally freezing environments [25,62]. These updates to SUTRA will soon be publicly available. For the present study, the boundary conditions and other parameters in the model are adjusted so that the simulations are performed for one-dimensional flow and heat transport with fully saturated conditions and spatiotemporally-constant Darcy velocity. In this case, SUTRA's governing heat transport equation reduces to Eq. (16) in the thawed zone. Fig. 2 shows the simulation domain, initial conditions, and boundary conditions employed in SUTRA. The constant Darcy velocity was established with specified fluid flux boundary conditions at the top (recharge) and bottom (discharge). As previously noted, the pore water velocity is higher in the frozen zone due to the pore ice reducing the effective porosity of the porous medium, but the Darcy velocity is spatiotemporally constant in both zones. Fully saturated conditions were maintained in SUTRA by applying uniform initial pressures of 0 Pa (Fig. 2).

The relationship between subzero temperatures and the volume of unfrozen water existing in the pore space is given by the soil freezing curve. Kurylyk and Watanabe [17] provide details for the process of applying capillary theory and the Clapeyron equation to develop a soil freezing curve from a previously established soil moisture characteristic curve for unfrozen soils. Other researchers have developed empirical soil freezing curves directly from

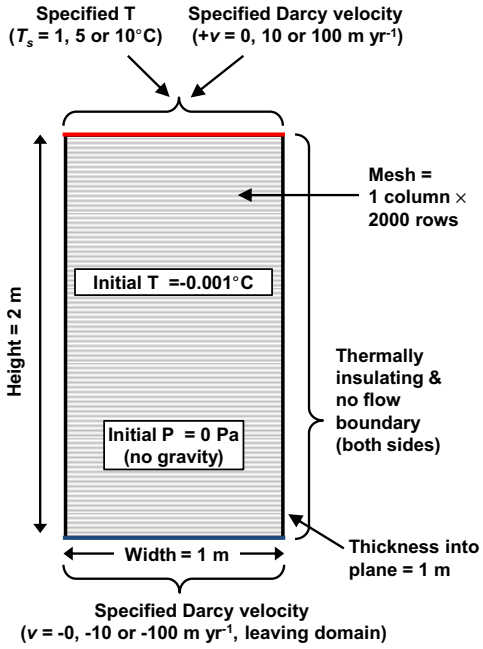

Fig. 2. Model domain, initial conditions, and boundary conditions employed in SUTRA. The no-flow, thermally insulating boundaries constrained the fluid flow and energy transport to the vertical direction. Water enters the domain at the upper boundary and discharges at the lower boundary. The domain was spatially discretized into one column of 2000 elements with a height of 1 mm (finer mesh than indicated).

laboratory tests conducted on soil samples e.g., [63,64]. Hence, SUTRA and other cold region thermohydraulic models generally utilize some form of a soil freezing curve that considers freezing over a range of temperatures less than 0 °C. However, the previously detailed analytical solutions employ the crude assumption that the soil freezing curve is represented as a step function. It is difficult to employ a step function soil freezing curve in a numerical model because the apparent heat capacity in the zone of freezing or thawing is dependent on the slope of the soil freezing curve [4,5], which would be infinite for a step function. A very steep piecewise linear soil freezing curve was employed in SUTRA to approximate a saturated step function soil freezing curve:

$$S_w = \begin{pmatrix} 1 & \text{if } T > T_f \\ 1 + b(T - T_f) & \text{if } T_{res} \leqslant T \leqslant T_f \\ S_{res} & \text{if } T < T_{res} \end{pmatrix} \quad (38)$$

where S_w is the total liquid water saturation (volume of unfrozen water/pore volume), b is the slope of the freezing curve ($b = (1 - S_{res})/(T_f - T_{res})$, $^\circ C^{-1}$), S_{res} is the residual liquid water saturation, and T_{res} is the residual freezing temperature (°C), which is the temperature at which S_{res} first occurs.

A very steep freezing curve (T_{res} very close to 0 °C, see Fig. 3) can approximate the infinitesimal freezing temperature range assumption of the Neumann, Lunardini, and Stefan solutions and the initial conditions of the Stefan and Lunardini solutions. For example, if T_{res} is assigned a value very close to 0 °C, the initial temperatures in the numerical model can be set very close to 0 °C (e.g., at or just below T_{res}) and still be cold enough to force the entire domain to be fully frozen at the beginning of the simulation and thus approximately match the conditions presented in Fig. 1. Note that very small time steps must be employed with a steep soil freezing curve, as coarse time steps could produce temperature changes that are larger than the freezing temperature range. In this case, no latent heat would be absorbed due to pore ice thaw, and the thawing front penetration would be over-predicted. Thus there is a tradeoff between assigning increasingly steep soil freezing curves and minimizing simulation time.

Note that the term representing liquid water saturation that experienced phase change S_{wf}, which is employed in the analytical solutions, can be related to the saturation terms employed in Eq. (38).

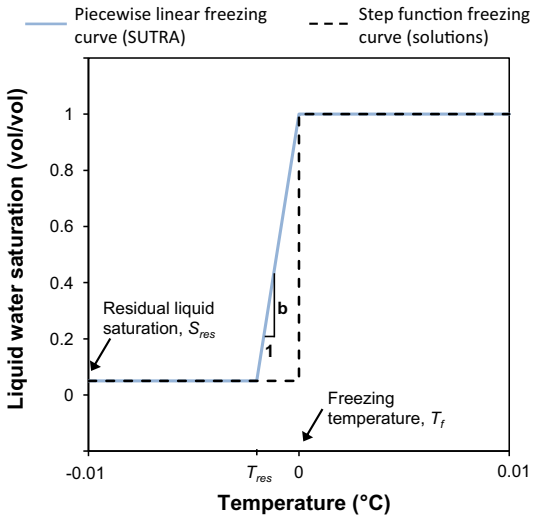

Fig. 3. Steep piecewise linear soil freezing curve (liquid water content vs. temperature) employed in SUTRA to mimic the step function soil freezing curve assumed by all three analytical solutions. The physical meaning of T_{res}, T_f, S_{res}, and b is outlined in the text, and Table A1 lists the values assigned to these parameters for the present study.

$$S_{wf} = S_w - S_{res} \quad (39)$$

The bulk thermal conductivity λ_{bulk} for both the analytical solutions and the SUTRA simulations is calculated as the volumetrically weighted arithmetic average of the thermal conductivities of the matrix constituents:

$$\lambda_{bulk} = (1 - \varepsilon)\lambda_s + \varepsilon S_w \lambda_w + \varepsilon S_i \lambda_i \quad (40)$$

where λ_s, λ_w, and λ_i are the thermal conductivities of the solid grain particles, liquid water, and ice respectively ($Wm^{-1}\,^\circ C^{-1}$), S_i is the pore ice saturation (volume of ice/pore volume), and other terms have been defined. In the fully thawed zone and for saturated conditions, the bulk thermal conductivity (simply given as λ elsewhere in this research) simplifies to:

$$\lambda = (1 - \varepsilon)\lambda_s + \varepsilon \lambda_w \quad (41)$$

The bulk heat capacity of the medium ($c\rho$) is taken as the weighted arithmetic average of the heat capacities of the matrix constituents. In the thawed zone and for saturated conditions, this simplifies to:

$$c\rho = (1 - \varepsilon)c_s \rho_s + \varepsilon c_w \rho_w \quad (42)$$

where c_s is the specific heat of the solid grain particles ($J\,kg^{-1}\,^\circ C^{-1}$) and ρ_s *is* the density of the solid grain particles ($kg\,m^{-3}$).

Table A1 in the appendix gives the numerical model input parameters utilized in the present study. Note that the SUTRA and analytical solution results presented herein can be reproduced in other codes that do not employ a weighted arithmetic mean for calculating bulk thermal conductivity provided that the resultant bulk thawed zone thermal conductivity and thermal diffusivity match those utilized in our simulations (Table A1). In general, the soil thermal properties represent those of a saturated sand with varying porosity [65]. The Lunardini solution assumes that the Darcy velocity is uniform throughout the entire domain (thawed and frozen); thus, for benchmarking purposes, any reduction in hydraulic conductivity due to pore ice formation is ignored. This is a simplification of the hydraulic dynamics in frozen or partially-frozen soils that facilitates benchmarking comparison. The value for permeability is not presented as it only affected the pressure distribution, not the temperature distribution, given the saturated conditions and the specified fluid flux boundary conditions at the top and bottom of the domain (Fig. 2).

Several piecewise linear soil freezing curves (i.e., different values for b and T_{res}) were considered, and the soil freezing curve parameterization indicated in Table A1 was shown to perform well for the thawing scenarios considered in this study. Due to the very steep freezing curve employed ($T_{res} = -0.0005$ °C, Table A1) very small time steps were required (minimum size = 0.00001 h). Simulations were performed for 20 days, thus requiring a large number of time steps (~7,000,000). However, due to the small number of nodes (4000, Fig. 2), the simulations were completed in approximately 15 h of computational time on a Dell Precision Workstation T7500 with a 4 core 2.67 GHz processor. A mesh and time-step refinement study was conducted to ensure that the SUTRA results were not significantly impacted by spatiotemporal discretization errors. Smaller time steps did not produce considerably better fits to the analytical solutions, and the spatial discretization error is minimal given the fine spatial resolution (1 mm).

Table 1 contains the details that differentiate the fifteen thawing scenarios considered in this study. Analytical solution calculations and numerical model simulations were performed for thawing scenarios with varying porosities, surface temperatures, and Darcy velocities. Varying soil properties (i.e., Stefan numbers) were considered to test the accuracy of the Lunardini solution with negligible flow against the exact Neumann solution. Various Darcy velocities were considered to examine the influence of heat

Table 1
Details for the simulations performed using the described analytical solutions and numerical model.

Thawing scenario/run	Analytical solutions	Compared to SUTRA (Y/N?)	Porosity	T_s (°C)	Darcy velocity (m yr^{-1})	Associated figures
1	Stefan, Neum., Lun.[a]	No	0.25	1	0[b]	4a, 5, 6a[b]
2	Stefan, Neum., Lun.	No	0.25	5	0	4a, 5
3	Stefan, Neum., Lun.	No	0.25	10	0	4a, 5, 6b
4	Stefan, Neum., Lun.	No	0.50	1	0	4b, 5, 6a
5	Stefan, Neum., Lun.	No	0.50	5	0	4b, 5
6	Stefan, Neum., Lun.	No	0.50	10	0	4b, 5, 6b
7	Lunardini	No	0.25	1	10	6a
8	Lunardini	No	0.25	1	100	6a
9	Lunardini	**Yes**	0.50	1	10	6a,8a
10	Lunardini	**Yes**	0.50	1	100	6a, 8b
11	Lunardini	No	0.25	10	10	6b
12	Lunardini	No	0.25	10	100	6b
13	Lunardini	No	0.50	10	10	6b
14	Lunardini	No	0.50	10	100	6b
15	Neumann	**Yes**	0.50	5[c]	0	7

[a] 'Neum'. = Neumann solution and 'Lun.' = Lunardini solution.
[b] In general, we list thawing scenarios together that had null (0 m yr^{-1}) and negligible (0.001 m yr^{-1}) Darcy velocities.
[c] Unlike every other thawing scenario given in Table 1, run 15 had initial temperatures much less than 0 °C (−5 °C).

advection on soil thawing and to form benchmarks to assess the performance of cold regions subsurface flow and heat transport models. In the cases of negligible or no Darcy velocity, the results between the three analytical solutions (Stefan, Neumann, and Lunardini) were compared. Table 1 also notes the instances that the results from the analytical solutions were compared to those obtained from the SUTRA simulations.

4. Results and discussion

4.1. Comparison of Stefan, Neumann, and Lunardini solutions for zero or negligible Darcy velocity

Fig. 4 shows the calculated depths to the thawing front obtained from each of the analytical solutions (Stefan, Neumann, and Lunardini) for six different thawing scenarios resulting from two porosities and three specified surface temperatures (runs 1–6, Table 1). The Stefan and Neumann solutions assume zero fluid flux, thus a very low Darcy velocity (v = 0.001 m yr^{-1}) was assigned for the Lunardini solution as the solution becomes unstable for the case of v and v_t = 0. A range of values for the low Darcy velocity were tested, and the results indicate that this Darcy velocity (v = 0.001 m yr^{-1}) is low enough to cause any advective influences to be negligible for the thawing scenarios considered. The Stefan and Lunardini solution results converge for low velocities, and they are thus represented with one series.

Fig. 4 demonstrates that the depth to the thawing front increases with increasing specified surface temperature and decreasing soil porosity (i.e., decrease in latent heat absorbed during thawing). Conversely, the accuracies of the Lunardini and Stefan solutions in comparison to the exact Neumann solution (error measured as a % of X) clearly decrease with increasing specified surface temperature and decreasing soil porosity (Fig. 4). It should be noted that, in addition to reducing the amount of pore ice available for phase change, decreasing the soil porosity

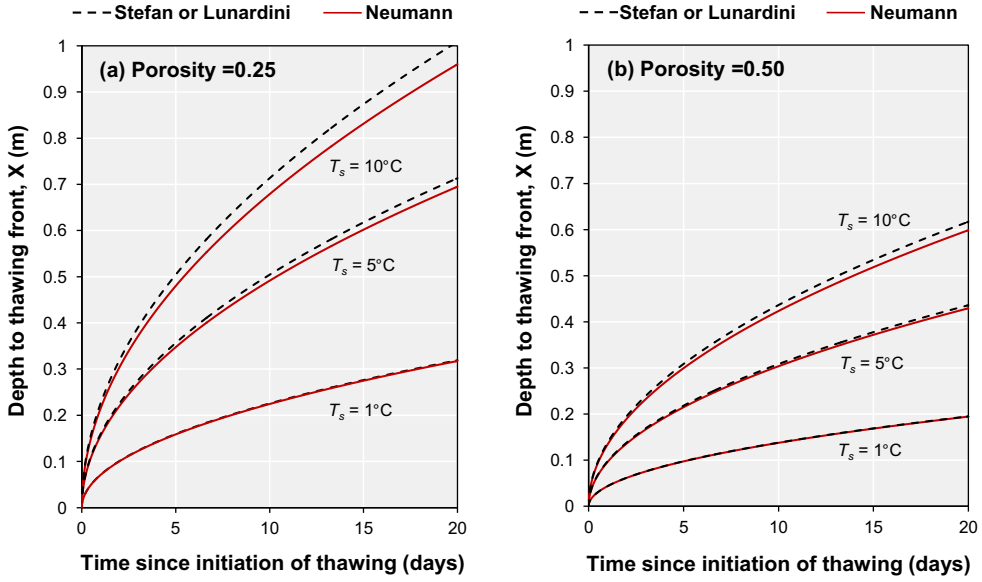

Fig. 4. Depth to the thawing front vs. the duration of thawing for (a) porosity = 0.25 (runs 1–3, Table 1), and (b) porosity = 0.5 (runs 4–6) calculated by the Stefan (Eq. (6)), Neumann (with T_i = 0 °C, Eqs. (12), (13) and (15)), and Lunardini (v = 0.001 m yr^{-1}, Eq. (33)) solutions. The Lunardini and Stefan solutions converge for all runs shown in this figure given the null or negligible Darcy velocity. Simulations were performed with three specified surface temperatures T_s (1, 5, and 10 °C). Thermal properties are indicated in Table A1.

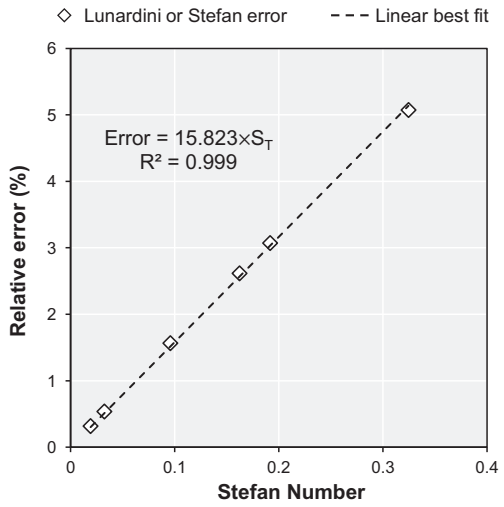

Fig. 5. The relative errors (%) in the approximate Stefan and Lunardini solutions (based on the exact solution of Neumann) after 20 days of thawing vs. the Stefan number (Eq. (7)) for the six thawing scenarios (runs 1–6) shown in Fig. 4. The best fit line with a zero intercept and the associated R^2 value are indicated.

increases the bulk thawed zone thermal diffusivity via Eqs. (41) and (42) given that the soil grains generally have a higher thermal conductivity and lower heat capacity than water. Both processes (i.e., increased thermal diffusivity and reduced latent heat) increase the rate of the thawing front penetration.

Fig. 5 more specifically shows that the Stefan and Lunardini solutions' errors increase with increasing Stefan number. The coefficient of determination (R^2 value) in Fig. 5 demonstrates that the relative errors of these approximate solutions vary linearly with the Stefan number. The relative error of the Lunardini solution after 20 days for the thawing scenario with $T_s = 1$ and porosity = 0.50 is only 0.32%. These results suggest that the Lunardini solution can be sufficiently accurate to be utilized for benchmarking purposes and that appropriate benchmark thawing scenarios (i.e., Stefan numbers) can be identified via comparison to the Neumann solution.

4.2. Lunardini solution with advection

The Lunardini solution results presented above have assumed negligible Darcy velocities and heat advection to facilitate comparison to the other solutions. Fig. 6 shows the impact of Darcy velocities up to 100 m yr^{-1} (positive implies recharge) calculated with the Lunardini solution for specified surface temperatures of 1 and 10 °C and porosities of 0.25 and 0.5 (runs 1, 3, 4, and 6–14, Table 1). The advective influence increases with decreasing porosity and increasing surface temperature, Darcy velocity, and time. For example, in Fig. 6(b), the thawing front penetration is approximately a linear function of time for a surface temperature of 10 °C, a porosity of 0.25, and a Darcy velocity of 100 m yr^{-1}. This linear relationship is indicative that the thawed zone thermal regime is advection-dominated given that conduction-dominated regimes exhibit curvature in the X-time relationship for this type of soil thawing problem (e.g., Fig. 4). Eq. (37) can be applied to demonstrate that the thawed zone advective flux is first equal to the conductive flux when $X = 0.37$ ($t = 1.53$ days) for this thawing scenario (run 12, Table 1).

For a porosity of 0.25 and a specified surface temperature of 10 °C (Fig. 6(b)), the differences between depths to the thawing front obtained for Darcy velocities of 0.001 and 100 m yr^{-1} is 1921 mm after 20 days. This difference decreases to 59 mm when the porosity is increased to 0.5 and the surface temperature is decreased to 1 °C (Fig. 6(a)). Note that a Darcy velocity of 100 m yr^{-1} is higher than the mean annual infiltration rates experienced in cryogenic soils; however, snowmelt-filled depressions overlying frozen soil can provide the source water for temporarily enhanced infiltrations rates that can be on the order of 10 m yr^{-1}[66].

The increase of the thermal influence of advection with time is expected given that the average thawed zone advective flux is temporally invariant while the thermal gradient and the conductive flux decrease as the depth to the thawing zone increases. The direct relationship between the surface temperature and the impact of advection is more complicated as the average thawed zone conductive and advective fluxes are both dependent on the surface temperature (e.g., Eq. (36)). However, the conductive flux is also inversely proportional to the depth to the thawing front, which

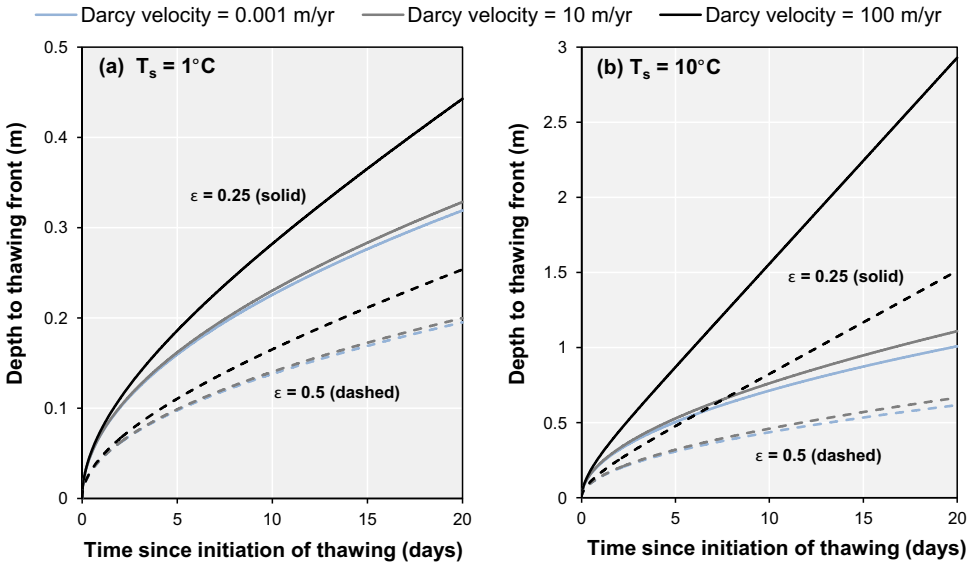

Fig. 6. Depth from surface to thawing front calculated by the Lunardini solution (Eq. (33)) versus time since initiation of thawing for (a) $T_s = 1$ °C (runs 1, 4 and 7–10, Table 1) and (b) $T_s = 10$ °C (runs 3, 6 and 11–14, Table 1). Results are shown for a porosity of 0.25 (solid lines) and 0.50 (dashed lines). The thermal influence of advection is indicated by examining three Darcy velocities: 0.001 m yr^{-1} (negligible advection), 10 m yr^{-1} and 100 m yr^{-1}. The thermal properties are indicated in Table A1. Note the difference in the vertical axis scale between the left and right panes.

increases with increasing surface temperature. Finally, the increase in the impact of the advective heat flux with decreasing porosity arises due to the dependency of the matrix volumetric heat capacity on porosity (Eq. (42)). For unfrozen saturated soils, the bulk volumetric heat capacity decreases with decreasing porosity because the volumetric heat capacity of most soil grains is less than the volumetric heat capacity of water [65]. Soils with lower heat capacities have less thermal inertia and will thus exhibit more thermal sensitivity to a given advective heat flux than soils with higher heat capacities.

4.3. Proposed benchmarks: comparison of the analytical solutions and numerical model

4.3.1. Comparison of Neumann solution and SUTRA

To date, the classic Neumann solution (Eqs. (12)–(14)) has not been utilized as a benchmarking solution in many existing cold regions subsurface water and energy transport models. The few studies that have employed this solution for verification and/or comparison purposes e.g., [6,46] have not presented sufficient details on the numerical model and analytical solution parameterization and/or results to enable other researchers to reproduce the same scenario for benchmarking purposes. Also, previous studies have used the solution to compute temperature profiles rather than the penetration of the soil thawing front. Here we present graphical and tabulated results obtained from the Neumann solution for the soil thawing front penetration when initial temperatures are below 0 °C. In this case, conduction occurs in both the thawed and frozen zones. Thus, unlike the Lunardini solution, the Neumann solution can calculate the influence of different thawed and frozen zone bulk soil thermal diffusivities. These differences can be significant, particularly for high porosity soils, as ice has a thermal diffusivity approximately eight times that of liquid water near 0 °C [65].

Fig. 7 shows the thawing front penetration simulated by SUTRA and the Neumann solution (Eqs. (12)–(14)) for a soil with an initial temperature of −5 °C, a specified surface temperature of 5 °C, and a soil porosity of 0.50 (run 15, Table 1). In this thawing scenario, the bulk thermal diffusivity of the frozen zone was 110% greater than the bulk thermal diffusivity of the thawed zone (Table A1). The maximum difference between the Neumann and SUTRA series in Fig. 7 is 0.99 mm, which is slightly less than the vertical spatial discretization of the SUTRA domain (1 mm).

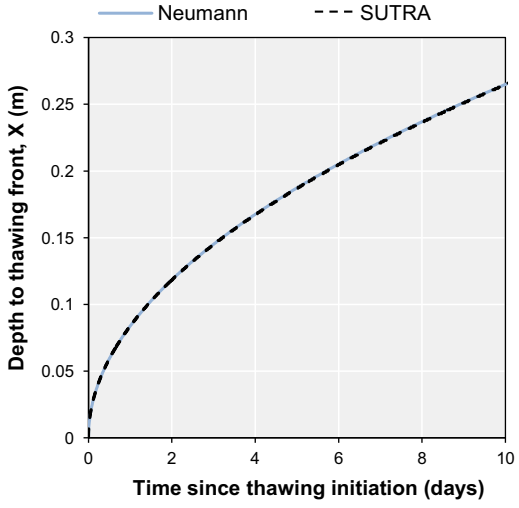

Fig. 7. Depth from surface to thawing front versus time since initiation of thawing for the Neumann solution (Eqs. (12)–(14)) and SUTRA for an initial temperature T_i of −5 °C, a porosity of 0.50, and a specified temperature T_s of 5 °C (run 15, Table 1). The thermal properties and other details regarding SUTRA's parameterization are provided in Table A1.

4.3.2. Comparison of Lunardini solution and SUTRA

SUTRA simulations were also compared to the Lunardini solution for scenarios with significant Darcy velocities. Fig. 8 shows the results obtained with the Lunardini solution and SUTRA for vertical downward Darcy velocities of 10 and 100 m yr^{-1} (runs 9 and 10, Table 1). Other thawing scenarios (e.g., higher surface temperatures, see Fig. 6) would better demonstrate the thermal influence of advection for these two Darcy velocities. However, the intent of these simulations is to illustrate the potential of the Lunardini solution to be employed as a benchmark solution, and thus we focus on thawing scenarios with low Stefan numbers and higher accuracies (Fig. 5). In Fig. 8, the differences between the depths to the thawing front obtained from the SUTRA simulations and the Lunardini solution after 20 days are −0.7 mm (−0.3% difference) for v = 10 m yr^{-1} and −1.6 mm (−0.6% difference) for v = 100 m yr^{-1}.

It is likely that the very minor differences between the Lunardini and SUTRA series arise due to both inaccuracies associated with the Lunardini solution and the numerical methods employed in SUTRA. For this Stefan number, the difference between the Neumann solution and the Lunardini solution with the Darcy velocity set to 0.001 m yr^{-1} is −0.6 mm (run 4, Table 1). Thus, the implicit errors in the Lunardini solution, which tends to slightly overestimate the thawing front penetration even at low Stefan numbers (Fig. 4), likely contributed to the noted differences between the SUTRA and Lunardini series in Fig. 8. As previously noted, *ad hoc* sensitivity analyses were conducted for the initial temperature, soil freezing curve parameters, and the spatiotemporal discretization. The SUTRA parameter values indicated in Table A1 produced results that can be compared to the Lunardini solution. In general, the very small differences obtained between the SUTRA and Lunardini results were deemed to be acceptable given the approximate nature of the Lunardini solution.

It should be noted that there is some ambiguity as to the location of X in the numerical model simulations. The transition between freezing and thawing occurs over a spatial range because pore ice thawing occurs between temperatures T_f and T_{res} (Table A1). In all of the SUTRA results graphically presented in this paper, the depth to the thawing front (X, Fig. 1) was taken as the location where temperature was first less than 0 °C. This represents the top of the partially frozen zone. The position where the simulated matrix temperature first equals the residual freezing temperature is the bottom of the partially frozen zone. Due to the steep freezing curve employed, the thickness of this partially frozen zone was at most 5 mm in the simulations shown in Fig. 8.

4.3.3. Recommended benchmarks

Appropriate benchmarks can be selected from the fifteen thawing scenarios presented in this paper (Table 1). Firstly, we recommend that the Neumann solution simulation with initial temperatures less than 0 °C (run 15, Table 1 and Fig. 7) be incorporated as a standard benchmark solution due to its ability to accommodate differences between the thermal diffusivities of the thawed and frozen zones. The Neumann solution results for this thawing scenario are tabulated for a duration of 20 days with an interval of 0.01 days in Table S1 of the supplementary material ('recommended benchmark 1').

A noted limitation of only employing the Neumann solution as a benchmark is that advection is not considered. This limitation can be overcome by utilizing both the Neumann and Lunardini solutions as benchmarks. We therefore recommend the thawing scenarios presented in Fig. 8 (v = 10 and 100 m yr^{-1}, runs 9 and

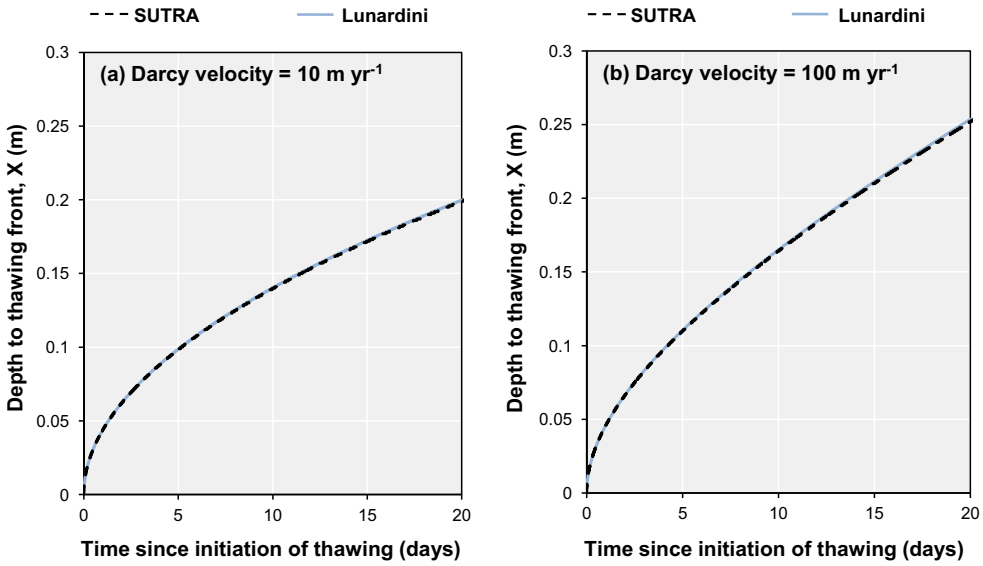

Fig. 8. Depth from surface to thawing front versus time since initiation of thawing calculated by the Lunardini solution (Eq. (33)) and SUTRA for a porosity of 0.50, a specified temperature T_s of 1 °C, and for Darcy velocities of (a) 10 m yr^{-1} (run 9, Table 1) and (b) 100 m yr^{-1} (run 10, Table 1). Domain thermal properties and other details regarding SUTRA's parameterization are provided in Table A1.

10, Table 1) as the Lunardini benchmark problems. These particular scenarios are proposed because the Lunardini solution has been shown to be reasonably accurate for this Stefan number (0.019, Fig. 5). The SUTRA results matched the Lunardini solution slightly better for $v = 10$ m yr^{-1} (run 9), but the influence of advection is more pronounced for $v = 100$ m yr^{-1} (run 10). The Lunardini solution results for these thawing scenarios are tabulated for a duration of 20 days with an interval of 0.01 days in Table S1 of the supplementary material ('recommended benchmarks 2 and 3').

5. Summary and conclusions

Cold regions subsurface flow and heat transport models are replete with differences in their underlying physics and numerical solution methods. In the past, few benchmark problems have been proposed to form inter-code comparisons, and these benchmarks have rarely been solved with more than one code. Furthermore, previously proposed analytical solution benchmarks for these models ignore the thermal influence of water flow. However, the primary advancement in recent cold regions subsurface heat transport modeling is the inclusion of water flow and associated heat advection. The Lunardini solution is particularly well-suited for a benchmark solution for these cold regions flow and heat transport models. To our knowledge, it is the only published analytical solution that accommodates conduction, advection, and pore water phase change without invoking the limiting assumption that the water flux is proportional to the rate of thaw. Assuming that the water flux is proportional to the rate of thaw simplifies the mathematical solution process [36,37], but this approach makes the problem more difficult to reproduce with numerical models.

This study has provided the first detailed derivation of the Lunardini solution and discussed the limitations associated with the steady-state assumption. In particular, we have demonstrated (via comparisons to the exact Neumann solution) that the Lunardini solution is accurate in the case of negligible water flow provided that the Stefan number is low. For realistic soil porosities and thermal conductivities, low Stefan numbers can primarily be achieved by specifying a low (albeit still >0 °C) surface temperature boundary condition. For the soil thermal properties considered in this study, the Lunardini solution relative error is only −0.32% after 20 days for a surface temperature of 1 °C, negligible Darcy velocity, and a porosity of 0.5. Furthermore, we have demonstrated via comparison to numerical modeling results that, in the case of significant water flow, the Lunardini solution can still produce reasonably accurate results. For instance, for the thawing scenario having a Darcy velocity of 10 m yr^{-1} and a surface temperature of 1 °C, the difference between the numerical results and the Lunardini solution after 20 days was −0.3% (−0.7 mm).

We recommend that the Lunardini scenarios with $v = 10$ and 100 m yr^{-1} (Fig. 8 and Table S1, supplementary material) be implemented as standard benchmarks for assessing the performance of subsurface water flow and heat transport models that include pore water phase change. We also recommend that future benchmarking initiatives include the Neumann solution example provided with initial temperatures less than 0 °C (Fig. 7 and Table S1, supplementary material), as this scenario accommodates different thermal diffusivities in the thawed and frozen zones. Future benchmarking initiatives e.g., [40] will likely also employ complex numerical solutions that more fully test the underlying equations and numerical solution methods of emerging cold regions water flow and energy transport simulators. However, analytical solutions remain a valuable component of benchmarking exercises because they eliminate errors associated with numerical solution methods and thus create a standard that is independent of any particular model.

Acknowledgments

We thank Editor D. Andrew Barry and four anonymous reviewers for their recommendations which improved the quality of this contribution. Alden Provost of the U.S. Geological Survey provided many valuable suggestions for this paper, particularly regarding the selection and derviation of the appropriate Lunardini solution for benchmarking. B.L. Kurylyk was funded by Natural Sciences and Engineering Research Council of Canada postgraduate scholarships (Julie Payette PGS and CGSD3), the Canadian Water Resources Association Dillon Scholarship, and an O'Brien Fellowship.

Table A1
Input parameters for SUTRA and the analytical solutions.

Parameter	Symbol	Value	Units
Hydraulic properties			
Porosity	ε	0.50 (0.25)[a]	–
Relative permeability [b]	k_{rel}	off	–
Darcy velocity (downwards)	v	0, 0.001, 10, and 100	m yr^{-1}
Gravity	g	0	m s^{-2}
Water saturation (total)	S_w	1	–
Sat. that undergoes phase change ($S_w - S_{res}$)	S_{wf}	1 (for solutions)	–
Thermal properties			
Thermal conductivity of thawed zone	λ	1.839 (2.458)	W m^{-1} °C^{-1}
Heat capacity of thawed zone	$c\rho$	3.201×10^6 (2.711×10^6)	J m^{-3} °C^{-1}
Thermal diffusivity of thawed zone	α	5.743×10^{-7} (9.067×10^{-7})	m^2 s^{-1}
Thermal diffusivity of frozen zone	α_f	1.205×10^{-6} (1.297×10^{-6})	m^2 s^{-1}
Thermal dispersivity	–	0[c]	m
Density of water	ρ_w	1000	kg m^{-3}
Specific heat of water	c_w	4182	J kg^{-1} °C^{-1}
Heat capacity of water	$c_w\rho_w$	4.182×10^6	J m^{-3} C^{-1}
Latent heat of fusion for water	L_f	334,000	J kg^{-1}
Other thermal settings			
Initial temperature	T_i	0[d]	°C
Freezing temperature (solutions)	T_f	0	°C
Residual freezing temperature (SUTRA)	T_{res}	−0.0005[e]	°C
Residual liquid saturation	S_{res}	0.0001	–
Slope of freezing function	b	1999.8	°C^{-1}
SUTRA solver settings and spatiotemporal discretization			
SUTRA element height	–	0.001	m
Number of time steps to 20 days	–	~7,000,000	–
SUTRA time step size	–	0.00001–0.0001	h

[a] Where applicable here and in other rows in this table, the first value given is for a porosity of 0.50, whereas the value in parentheses is for a porosity of 0.25.
[b] Note that because a water flux is specified at the top and bottom of the model and the medium was saturated (Fig. 2), the actual permeability is irrelevant. For the sake of simplicity, we assumed no reduction in permeability due to pore ice formation.
[c] Thermal dispersivity is a parameter included in many models of coupled subsurface water flow and energy transport. Thermal dispersion is a thermal homogenizing process that arises due to the tortuous flow path traveled by groundwater [67]. This phenomenon is not considered in the analytical solutions, and thus thermal dispersivity was set to zero.
[d] The initial temperature for each of the analytical simulations was set to 0 °C (except for one Neumann solution run that had a T_i of −5 °C, run 15, Table 1 and Fig. 6). The initial temperature could not be set at exactly 0 °C in SUTRA, or the medium would be initially fully thawed. Thus the initial temperature was set at a value (−0.001 °C) slightly below the residual freezing temperature T_{res}.
[e] The complete freezing temperature (i.e. the temperature at residual liquid water saturation due to freezing) was increased to −0.01 °C for the SUTRA runs to match the Neumann solution with initial temperatures of −5 °C (Fig. 6). This increase was required because the higher surface temperature in this run (5 °C) in comparison to the surface temperatures of other runs (1 °C) caused soil thawing that was too rapid given the initially small time step.

Appendix A

Contains Table A1.

Appendix B. Supplementary data

Supplementary data associated with this article can be found, in the online version, at http://dx.doi.org/10.1016/j.advwatres.2014.05.005.

References

[1] Bense VF, Ferguson G, Kooi H. Evolution of shallow groundwater flow systems in areas of degrading permafrost. Geophys Res Lett 2009;36:L22401. http://dx.doi.org/10.1029/2009GL039225.
[2] Painter S. Three-phase numerical model of water migration in partially frozen geological media: model formulation, validation, and applications. Comput Geosci 2011;15:69–85. http://dx.doi.org/10.1007/s10596-010-9197-z.
[3] Rowland JC, Travis BJ, Wilson CJ. The role of advective heat transport in talik development beneath lakes and ponds in discontinuous permafrost. Geophys Res Lett 2011;38:I7. http://dx.doi.org/10.1029/2011GL048497.
[4] McKenzie JM, Voss CI, Siegel DI. Groundwater flow with energy transport and water–ice phase change: numerical simulations, benchmarks, and application to freezing in peat bogs. Adv Water Resour 2007;30:966–83. http://dx.doi.org/10.1016/j.advwatres.2006.08.008.
[5] Hansson K, Simunek J, Mizoguchi M, Lundin LC, van Genuchten MT. Water flow and heat transport in frozen soil: numerical solution and freeze-thaw applications. Vadose Zone J 2004;3:693–704. http://dx.doi.org/10.2136/vzj2004.0693.
[6] Dall'Amico M, Endrizzi S, Gruber S, Rigon R. A robust and energy-conserving model of freezing variably-saturated soil. Cryosphere 2011;5:469–84. http://dx.doi.org/10.5194/tc-5-469-2011.
[7] Sheshukov AY, Nieber JL. One-dimensional freezing of nonheaving unsaturated soils: model formulation and similarity solution. Water Resour Res 2011;47:W11519. http://dx.doi.org/10.1029/2011WR010512.
[8] White MD, Oostrom M. STOMP Subsurface transport over multiple phases: users guide. Pacific Northwest National Laboratory, PNNL-15782; 2006. 120pp.
[9] Liu Z, Yu X. Coupled thermo-hydro-mechanical model for porous materials under frost action: theory and implementation. Acta Geotech 2011;6:51–65. http://dx.doi.org/10.1007/s11440-011-0135-6.
[10] Endrizzi S, Gruber S, Dall'Amico M, Rigon R. GEOtop 2.0: simulating the combined energy and water balance at and below the land surface accounting for soil freezing, snow cover, and terrain effects. Geosci Model Dev Discuss 2013;6:6279–314. http://dx.doi.org/10.5194/gmdd-6-6279-2013.
[11] Tan X, Chen W, Tian H, Cao J. Water flow and heat transport including ice/water phase change in porous media: numerical simulation and application. Cold Reg Sci Technol 2011;68:74–84. http://dx.doi.org/10.1016/j.coldregions.2011.04.004.
[12] Karra S, Painter SL, Lichtner PC. Three-phase numerical model for subsurface hydrology in permafrost-affected regions. Cryosphere Discuss 2014;8:145–85. http://dx.doi.org/10.5194/tcd-8-149-2014.
[13] Coon ET, Berndt M, Garimella R, Mouton JD, Painter S. A flexible and extensible mutli-process simulation capability for the terrestrial Arctic. Frontiers in computational physics: modeling the earth system. Boulder, Co; 2012.
[14] Jiang Y, Zhuang Q, O'Donnell JA. Modeling thermal dynamics of active layer soils and near-surface permafrost using a fully coupled water and heat transport model. J Geophys Res – Atmos 2012;117:D11110. http://dx.doi.org/10.1029/2012JD017512.
[15] Grenier C, Regnier D, Mouche E, Benabderrahmane H, Costard F, Davy P. Impact of permafrost development on groundwater flow patterns: a numerical study considering freezing cycles on a two-dimensional vertical cut through a generic river-plain system. Hydrogeol J 2013;21:257–70. http://dx.doi.org/10.1007%2Fs10040-012-0909-4.

[16] Kelleners TJ. Coupled water flow and heat transport in seasonally frozen soils with snow accumulation. Vadose Zone J 2013:12. http://dx.doi.org/10.2136/vzj2012.0162.
[17] Kurylyk BL, Watanabe K. The mathematical representation of freezing and thawing processes in variably-saturated, non-deformable soils. Adv Water Resour 2013;60:160–77. http://dx.doi.org/10.1016/j.advwatres.2013.07.016.
[18] Watanabe K, Wake T. Hydraulic conductivity in frozen unsaturated soil. In: Kane DL, Hinkel KM, editors. Proceedings of the ninth international conference on permafrost. Fairbanks, Alaska: University of Alaska; 2008. p. 1927–32.
[19] Tarnawski VR, Wagner B. On the prediction of hydraulic conductivity of frozen soils. Can Geotech J 1996;33:176–80. http://dx.doi.org/10.1139/t96-033.
[20] Azmatch TF, Sego DC, Arenson LU, Biggar KW. Using soil freezing characteristic curve to estimate the hydraulic conductivity function of partially frozen soils. Cold Reg Sci Technol 2012;83–84:103–9. http://dx.doi.org/10.1016/j.coldregions.2012.07.002.
[21] Lundin L. Hydraulic properties in an operational model of frozen soil. J Hydrol 1990;118:289–310. http://dx.doi.org/10.1016/0022-1694(90)90264-X.
[22] McKenzie JM, Voss CI. Permafrost thaw in a nested groundwater-flow system. Hydrogeol J 2013;21:299–316. http://dx.doi.org/10.1007/s10040-012-0942-3.
[23] Frampton A, Painter SL, Destouni G. Permafrost degradation and subsurface-flow changes caused by surface warming trends. Hydrogeol J 2013;21:271–80. http://dx.doi.org/10.1007/s10040-012-0938-z.
[24] Bense VF, Kooi H, Ferguson G, Read T. Permafrost degradation as a control on hydrogeological regime shifts in a warming climate. J Geophys Res 2012;117:F03036. http://dx.doi.org/10.1029/2011JF002143.
[25] Kurylyk BL, MacQuarrie KTB, Voss CI. Climate change impacts on the temperature and magnitude of groundwater discharge from small, unconfined aquifers. Water Resour Res 2014;50:3253–74. http://dx.doi.org/10.1002/2013WR014588.
[26] Quinton WL, Baltzer JL. The active-layer hydrology of a peat plateau with thawing permafrost (Scotty Creek, Canada). Hydrogeol J 2013;21:201–20. http://dx.doi.org/10.1007%2Fs10040-012-0935-2.
[27] Wu Q, Zhang T, Liu Y. Thermal state of the active layer and permafrost along the Qinghai-Xizang (Tibet) Railway from 2006 to 2010. Cryosphere 2012;6:607–12. http://dx.doi.org/10.5194/tc-6-607-2012.
[28] Walvoord MA, Voss CI, Wellman TP. Influence of permafrost distribution on groundwater flow in the context of climate-driven permafrost thaw: Example from Yukon Flats Basin, Alaska, United States. Water Resour Res 2012;48:W07524. http://dx.doi.org/10.1029/2011WR011595.
[29] Connon RF, Quinton WL, Craig JR, Hayashi M. Changing hydrologic connectivity due to permafrost thaw in the lower Liard River valley, NWT, Canada. Hydrol Process 2014. http://dx.doi.org/10.1002/hyp.10206 [Online first].
[30] Subcommittee on Ground Freezing. Knowledge of frozen soil-technology of artificial frozen soil [Trans. from Japanese to English]. Seppyo 2014;72:179–92.
[31] Tan X, Weizhong C, Guojun W, Yang Y. Numerical simulations of heat transfer with ice-water phase change occurring in porous media and application to a cold-region tunnel. Tunn Underg Sp Tech 2013;38:170–9. http://dx.doi.org/10.1016/j.tust.2013.07.008.
[32] Grimm RE, Painter SL. On the secular evolution of groundwater on Mars. Geophys Res Lett 2009;36:L24803. http://dx.doi.org/10.1029/2009GL041018.
[33] Lunardini VJ. Heat transfer with freezing and thawing. New York (NY): Elsevier Science Pub. Co.; 1991.
[34] Kane DL, Hinzman LD, Zarling JP. Thermal response of the active layer to climatic warming in a permafrost environment. Cold Reg Sci Technol 1991;19:111–22. http://dx.doi.org/10.1016/0165-232X(91)90002-X.
[35] Jafarov EE, Marchenko SS, Romanovsky VE. Numerical modeling of permafrost dynamics in Alaska using a high spatial resolution dataset. Cryosphere 2012;6:613–24. http://dx.doi.org/10.5194/tc-6-613-2012.
[36] Nixon JF. The role of convective heat transport in the thawing of frozen soils. Can Geotech J 1975;12:425–529. http://dx.doi.org/10.1139/t75-046.
[37] Lunardini VJ. Effect of convective heat transfer on thawing of frozen soil. In: Lewkowicz AG, Allard M, editors. Proceedings of the seventh international conference on permafrost. Canada: Yellowknife; 1998. p. 689–95.
[38] Jumikis AR. Thermal soil mechanics. New Brunswick (NJ): Rutgers University Press; 1966.
[39] Lunardini VJ. Heat transfer in cold climates. New York: Van Nostrand Reinhold Co.; 1981.
[40] Grenier C, Roux N, Costard F. A new benchmark of thermo-hydraulic codes for cold regions hydrology. EGU Gen Assembly Conf Abstr 2013;15:3861.
[41] Stefan J. Uber die Theorie der Eisbildung, insbesondere uber die Eisbildung im Polarmee. Ann Phys Chem Neueu Folge 1891;42:269–86.
[42] Mitchell SL, Myers TG. Application of standard and refined heat balance integral methods to one-dimensional Stefan problems. SIAM Rev 2010;52:57–86. http://dx.doi.org/10.1137/080733036.
[43] Neumann F. Lectures given in the 1860s. Braunschweig; 1901 [See Weber HM Die partiellen Differentialgleichungen der mathematischen Physic nach Riemanns Vorlesungen].
[44] Aldrich HP, Paynter HM. Analytical studies of freezing and thawing in soils. US Army Corps of Engineers, First Interim, Report No. 42; 1953.
[45] Andersland OB, Anderson DM. Geotechnical engineering for cold regions. New York (NY): McGraw-Hill; 1978.
[46] Nakano Y, Brown J. Effect of a freezing zone of finite width on the thermal regime of soils. Water Resour Res 1971;7:1226–33. http://dx.doi.org/10.1029/WR007i005p01226.
[47] Lock GSH, Gunderson JR, Quon D, Donnelly JK. A study of one-dimensional ice formation with particular reference to periodic growth and decay. Int J Heat Mass Transfer 1969;12:1343–52. http://dx.doi.org/10.1016/0017-9310(69)90021-0.
[48] Lock GSH. On the perturbation solution of the ice-water layer problem. Int J Heat Mass Transfer 1971;14:642–4. http://dx.doi.org/10.1016/0017-9310(71)90013-5.
[49] Hayashi M, Goeller N, Quinton WL, Wright N. A simple heat-conduction method for simulating the frost-table depth in hydrological models. Hydrol Process 2007;21:2610–22. http://dx.doi.org/10.1002/hyp.6792.
[50] Nixon JF, McRoberts EC. A study of some factors affecting the thawing of frozen soils. Can Geotech J 1973;10:439–52. http://dx.doi.org/10.1139/t73-037.
[51] Cho SH, Sunderland JE. Phase-change problems with temperature-dependent thermal-conductivity. J Heat Transfer – Trans ASME 1974;96:214–7. http://dx.doi.org/10.1115/1.3450167.
[52] Changwei X, Gough WA. A simple thaw-freeze algorithm for a multi-layered soil using the Stefan equation. Permafrost Periglac 2013;24:252–60. http://dx.doi.org/10.1002/ppp.1770.
[53] Stallman RW. Steady one-dimensional fluid flow in a semi-infinite porous medium with sinusoidal surface temperature. J Geophys Res 1965;70:2821–7. http://dx.doi.org/10.1029/JZ070i012p02821.
[54] Domenico PA, Schwartz FW. Physical and chemical hydrogeology. New York: John Wiley and Sons Inc.; 1990.
[55] Kurylyk BL, MacQuarrie KTB. A new analytical solution for assessing projected climate change impacts on subsurface temperature. Hydrol Process 2013;60:160–77. http://dx.doi.org/10.1002/hyp.9861.
[56] Markle JM, Schincariol RA. Thermal plume transport from sand and gravel pits – potential thermal impacts on cool water streams. J Hydrol 2007;338:174–95. http://dx.doi.org/10.1016/j.jhydrol.2007.02.031.
[57] Fel'dman GM. Calculation of ground thawing allowing for water seepage. US Army Cold Regions Research and Engineering Laboratory Draft, Translation 334; 1972.
[58] Bredehoeft JD, Papadopulos IS. Rates of vertical groundwater movement estimated from the Earth's thermal profile. Water Resour Res 1965;1:325–38. http://dx.doi.org/10.1029/WR001i002p00325.
[59] Stewart J. Calculus concepts and contexts. 2nd ed. Pacific Grove (CA): Brooks/Cole; 2001.
[60] Ingebritsen SE, Sanford WE, Neuzil CE. Groundwater in geologic processes. 2nd ed. Cambridge, New York: Cambridge University Press; 2006.
[61] Voss CI, Provost AM. SUTRA: a model for saturated-unsaturated variable-density ground-water flow with solute or energy transport. US Geological Survey Water Resources Investigations, Report 02-4231; 2010.
[62] Briggs MA, Walvoord MA, McKenzie JM, Voss CI, Day-Lewis FD, Lane JW. New permafrost is forming around shrinking Arctic lakes, but will it last? Geophys Res Lett 2014;41:1585–92. http://dx.doi.org/10.1002/2014GL059251.
[63] Kozlowski T. A semi-empirical model for phase composition of water in clay-water systems. Cold Regions Sci Technol 2007;47:226–36. http://dx.doi.org/10.1016/j.coldregions.2007.03.013.
[64] Kozlowski T. Some factors affecting supercooling and the equilibrium freezing point in soil-water systems. Cold. Regions Sci Technol 2009;59:25–33. http://dx.doi.org/10.1016/j.coldregions.2009.05.009.
[65] Bonan G. Ecological climatology. 2nd ed. United Kingdom: Cambridge University Press; 2008.
[66] Hayashi M, van der Kamp G, Schmidt R. Focused infiltration of snowmelt water in partially frozen soil under small depressions. J Hydrol 2003;270:214–29. http://dx.doi.org/10.1016/S0022-1694(02)00287-1.
[67] Molina-Giraldo N, Bayer P, Blum P. Evaluating the influence of thermal dispersion on temperature plumes from geothermal systems using analytical solutions. Int JTherm Sci 2011;50:1223–31. http://dx.doi.org/10.1016/j.ijthermalsci.2011.02.004.